chemosensors

Article

A Sensitive Immunochromatographic Test Strip Based on Hydrophobic Quantum Dots Incorporated into Mg/Fe Nanoflowers for HCG Detection

Hao Liu [1], Qing Zhang [2], Ning Bao [3] and Shou-Nian Ding [1,*]

[1] Jiangsu Province Hi-Tech Key Laboratory for Bio-Medical Research, School of Chemistry and Chemical Engineering, Southeast University, Nanjing 211189, China
[2] Key Laboratory of Consumer Product Quality Safety Inspection and Risk Assessment for State Market Regulation, Chinese Academy of Inspection and Quarantine, Beijing 100176, China
[3] School of Public Health, Nantong University, Nantong 226019, China
* Correspondence: snding@seu.edu.cn

Abstract: As the most widely used disposable paper-based diagnostic tool in the world, immunochromatographic test strips (ICTS) have occupied more and more positions in the field of rapid diagnosis due to their ease of operation and affordability. Therefore, the development of an easily prepared, sensitive, and accurate signal reporter is of great significance for the detection of some low-abundance biomarkers in clinical diagnosis. Herein, Mg/Fe layered double hydroxide nanoflowers (MF NFs) were selected as adsorption templates and sulfhydryl-functionalized, followed by one-step loading of hydrophobic CdSe/ZnS quantum dots in the organic phase via a metal-thiol covalent bond. After coating the reporter with branched polyethyleneimine (PEI), a novel ICTS fluorescent reporter was prepared. The modification of PEI not only improved the hydrophilicity of MF@CdSe/ZnS NFs but also introduced amino functional groups on the surface of the reporter for subsequent conjugation with antibodies. X-ray photoelectron spectroscopy, UV-vis absorption, X-ray diffraction, fluorescence spectroscopy, and infrared spectroscopy were used to characterize the composition of MF@CdSe/ZnS NFs. Under the optimal experimental conditions, the detection range of MF@CdSe/ZnS@PEI-ICTS for the model analyte HCG was 0.1–500 mIU/mL, and the limit of detection (LOD) reached was 0.1 mIU/mL. The potential for practical application was validated by the detection of HCG in spiked healthy human serum, showing overall recoveries between 90.48 and 116.1% with coefficients of variation that ranged from 3.66 to 12.91%.

Keywords: layered double hydroxide nanoflowers; immunochromatography test strip; hydrophobic CdSe/ZnS QDs; human chorionic gonadotropin

Citation: Liu, H.; Zhang, Q.; Bao, N.; Ding, S.-N. A Sensitive Immunochromatographic Test Strip Based on Hydrophobic Quantum Dots Incorporated into Mg/Fe Nanoflowers for HCG Detection. *Chemosensors* **2023**, *11*, 114. https://doi.org/10.3390/chemosensors11020114

Academic Editor: Chunsheng Wu

Received: 8 November 2022
Revised: 30 December 2022
Accepted: 1 February 2023
Published: 3 February 2023

1. Introduction

POCT (point-of-care testing) is a test that can be performed on site or nearby, according to medical and individual patient needs, without the constraints of place, time, testing environment, and testing facilities. POCT currently facilitates in vitro testing of various biological indicators, reduces the volume of samples tested, greatly shortens the turnaround time of samples tested, and allows for flexible and versatile application scenarios. As a well-known disposable paper-based diagnostic tool, immunochromatography test strips (ICTS) occupy an increasingly high position in the field of rapid diagnosis, so they are widely used in the qualitative, semi-quantitative, and even quantitative detection of various proteins and small molecules [1,2]. The initial design of ICTS was first reported by Plotz and Singer in 1956 and was widely employed in urine-based pregnancy recognition [3,4]. However, due to the limited detection sensitivity of colloidal gold-based ICTS, they are usually used to qualitatively detect some high-abundance biomarkers (>10^{-12} M), which largely limits the application of ICTS in the field of low-abundance biomarker detection. In the case of

the recent global COVID-19 pandemic, testing a single serological antibody or antigen can only indicate a person's past or recent exposure to SARS-CoV-2 and cannot identify the "hot spot" of infection and effectively control the disease in a timely manner. Therefore, multiple and extensive tests are necessary. Ideally, close contacts should be tested weekly or daily to be promptly isolated and to minimize the spread of the virus in the community. The main disadvantages of ICTS based on colloidal gold are low sensitivities, limited precision quantification abilities, and low detection sensitivities. As a result, some false-negative cases can be mistaken for being non-infectious, creating a significant risk of further spreading in the community. In addition to colorimetric methods, signal types used in ICTS include fluorescent reporters [5], phosphorescence reporters [6], magnetic signals [7], and electrochemical signals [8]. Among them, the fluorescent reporter provides better signal contrast and lower background interference, making it have higher sensitivity and lower detection limits for the same detection time. Therefore, the development of higher performance fluorescent labels will be of great benefit to ICTS in dealing with multiple and complex detection.

Among the fluorescence reporter molecules, colloidal quantum dots (QDs) have the advantages of wide absorption, a narrow emission band, size/shape, composition, and surface properties that can be controlled artificially and accurately, and their luminous efficiency is better than that of conjugated molecules (polymers) or inorganic phosphors [9,10]. Its applications in biomarkers, photovoltaic devices, and light-emitting diodes have been extensively and deeply studied [11–13]. Foubert et al. conducted a comparative study of colloidal gold and QDs as labels for multiplex screening assays for toxins, and the results showed that QDs-based ICTS consume fewer immunological reagents, have a lower-false negative rate (<5%), higher sensitivity, and better economic efficiency [14]. Deng et al. used QDs to detect miRNAs rapidly and sensitively, and the results showed that the detection method was also 10 times more sensitive than traditional colloidal gold-based miRNA detection test strips [15]. Although studies have pointed out that ICTS based on QDs is more sensitive than colloidal gold-based ICTS, it is still difficult to detect many low-abundance biomarkers [16,17]. Embedding QDs in large numbers into individual nanoparticles is a useful strategy for improving sensitivity [10,18,19]. At present, there are four main approaches: in situ self-assembly [20,21], in situ polymerization [22], layer-by-layer assembly [23], and porous nanoparticle-based incorporation [10,18]. Due to the presence of many alkyl stabilizers on the surface of QDs, this type of quantum dot can only be dispersed in non-polar solvents (chloroform, hexane, etc.). However, either in situ or template-based assembly processes require pre-capped ligand exchange for nanocrystals because these ligands on the surface of oil-soluble quantum dots are usually hydrophobic and lack reactive functional groups [24,25]. This process may cause irreversible physicochemical damage to QDs. Compared with the other three methods, the porous nanoparticle-based incorporation strategy has the advantages of high loading capacity, good uniformity, and reduced aggregation [26,27]. Several previous papers have demonstrated that nanoassemblies with high homogeneity and surface loading density can be prepared directly in the organic phase by ligand-driven assembly of metal-containing nanocrystals with thiol-capped colloids using metal-thiol covalent bonding [28–30]. For instance, Hu et al. fully used dendritic SiO_2 as templates to enrich high-density hydrophobic QDs for the ultrasensitive determination of C-reactive proteins [10].

Layered double hydroxides (LDHs) consist of stacked, positively charged, brucite-like octahedral metal hydroxide layers and interlayer anions and water molecules. It is a class of layered materials with positively charged metal hydroxide layers and charge-balancing anions [31]. In recent years, due to its low toxicity, unique layered structure, good biocompatibility, high anion exchange capacity, adjustable particle size, and other advantages, have been widely studied in the field of biomedicine [32,33]. LDH nanoparticles, especially spherical LDH particles with porous structures, have been proven to be excellent adsorbents due to their low cost, large specific surface area, and strong adsorption capacity [34–36]. Herein, for the first time, surface thiol-functionalized MF NFs (SH-MF)

were employed as adsorption templates to load hydrophobic CdSe/ZnS QDs in an oil-phase solvent. As illustrated in Figure 1, MF NFs were used as adsorption templates, and many hydrophobic CdSe/ZnS QDs were loaded via thiol-metal covalent bonding. It is necessary to transfer the MF@CdSe/ZnS NFs from the oil phase to the water phase. Some studies have shown that coating or embedding oil-phase nanocrystals with hydrophilic polymers is a feasible method to solve the above problems [37,38]. For example, Chen et al. developed a novel ICTS system of QDs-doped polystyrene nanoparticles with satisfactory recovery and reproducibility. The test strip can simultaneously detect cytokeratin-19 fragments and carcinoembryonic antigens in human serum, with limits of detection of 0.16 and 0.35 ng/mL, respectively. Therefore, it is completely feasible to use an optimized amount of branched polyethyleneimine (PEI) to modify the fluorescent reporter in this work. Finally, a novel high-density oil-phase CdSe/ZnS QD that incorporated MF NFs fluorescent signal reporters (MF@CdSe/ZnS@PEI) was successfully prepared. These nanoflowers were further bound to antibodies and successfully applied to the ICTS for the highly sensitive detection of HCG.

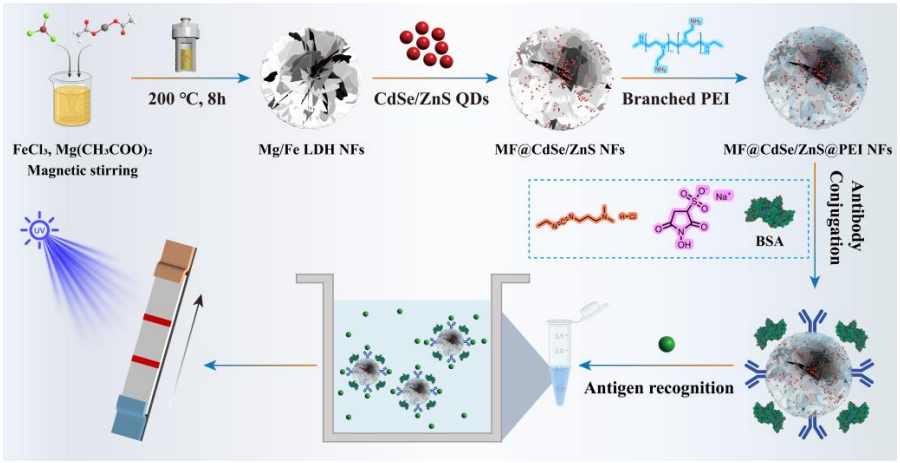

Figure 1. Schematic illustration of MF@CdSe/ZnS@PEI-ICTS for HCG detection.

2. Materials and Methods

2.1. Reagents and Characterization

Mg $(OAc)_2 \cdot 4H_2O$, $FeCl_3 \cdot 6H_2O$, ethylene glycol, Cd $(Ac)_2$, Zn $(Ac)_2$, ethanol, ammonia water, oleic acid (OA), selenium powder, sulfur powder, 1-octadecene KH_2PO_4, $Na_2HPO_4 \cdot 12H_2O$, NaCl, KCl, Tween-20, and $CHCl_3$ were purchased from Sinopharm Chemical Reagent Co., Ltd. Tri-n-octyl phosphine, γ-mercaptopropyltrimethoxysilane, EDC·HCl and Sulfo-NHS were purchased from Shanghai Aladdin Biochemical Technology Co., Ltd. (Shanghai, China). Carbohydrate antigen 125 (CA125), alpha fetoprotein (AFP), carbohydrate antigen 199 (CA199), and carcinoembryonic antigen (CEA) were purchased from Shanghai Linc-Bio Science Co., Ltd (Shanghai, China). The anti-α-HCG (Ab_1), anti-β-HCG (Ab_2), goat anti-mouse IgG antibodies, and the parts that make up the ICTS were purchased from Shanghai Joey Biotechnology Co. Ltd (city, country). All buffers in this work were prepared fresh at the time of use. A Bruker ASCENDTM 400WB spectrometer (Bruker, Newark, DE, USA) was used to characterize the ^{13}C CP/MAS NMR spectra of thiol-modified MF NFs at 400 MHz, reported in parts per million (ppm). UV-vis absorption spectra were obtained on a Shimadzu UV 2600 spectropolarimeter (Kyoto, Japan) and were used to characterize the absorbance values of hydrophobic CdSe/ZnS QDs, MF@CdSe/ZnS NFs, and MF@CdSe/ZnS@PEI NFs. Scanning electron microscope (SEM) photographs were taken under a field emission scanning electron microscope (Thermo Scientific, Waltham, MA, USA) operating at 20 kV to characterize MF NFs. Transmission electron microscopy (TEM) images were taken under a field emission high-resolution transmission electron microscope Talos F200X (Thermo Scientific, Waltham, MA, USA) for the characterization of hydrophobic CdSe/ZnS QDs, MF@CdSe/ZnS NFs, and MF@CdSe/ZnS

@PEI NFs, and elemental analysis. Fourier transform infrared (FT-IR) spectra were collected from a Nicolet 5700 (Thermo Nicolet Corporation, Waltham, MA, USA) infrared spectrometer with a characterization range of 4000–400 cm^{-1} for the characterization of Mg/Fe NFs, MF@CdSe/ZnS NFs, and MF@CdSe/ZnS@PEI NFs. Here, the surface potential characterization of hydrophobic CdSe/ZnS QDs, MF@CdSe/ZnS NFs, and MF@CdSe/ZnS@PEI NFs at 25 °C was performed using a Zetasizer Nano-ZS from Malvern Instruments (Malvern, UK). Powder X-ray diffraction (XRD) analysis of MF NFs and MF@CdSe/ZnS NFs was performed using a Rigaku Ultima IV multifunctional horizontal X-ray diffractometer (Rigaku, Tokyo, Japan). X-ray photoelectron spectroscopy (XPS, PreVac, Rogow, Poland) studies were performed using the XPS-2 system to characterize the elemental composition of MF NFs and MF@CdSe/ZnS NFs.

2.2. Preparation Procedures of the Red-Emitting Hydrophobic CdSe/ZnS QDs

The synthesis procedures for CdSe/ZnS QDs are based on previously reported literature with some minor changes [39]. An amount of 1.0 mmol Cd $(Ac)_2$ (Sinopharm Chemical, Shanghai, China) and 4.0 mmol Zn $(Ac)_2$ (Sinopharm Chemical) were placed in a four neck round bottom flask that contained 9 mL of OA (Sinopharm Chemical) and 10 mL of ODE (Sinopharm Chemical). The mixture was first heated to 180 °C to form a homogeneous solution, and after degassing at 150 °C, the mixture was heated to 300 °C. Then 0.4 mL of TOP-Se solution (1 M) was rapidly injected into the mixture solution first, and then 4 mL of TOP-S solution (1 M) was injected continuously at 30 s intervals. Finally, the temperature was set at 280 °C for subsequent growth.

2.3. Preparation Procedures of MF@CdSe/ZnS@PEI NFs [36]

An amount of 50.0 mg of MF NFs were uniformly dispersed in absolute ethanol, followed by 0.5 mL of ammonia water and 0.5 mL of γ-mercaptopropyltrimethoxysilane, and the mixture was homogeneously sonicated and vigorously stirred at room temperature for 6 hours. After the reaction, thiol-modified MF NFs (SH-MF) can be obtained by centrifugation. The SH-MF product was thoroughly washed alternately with absolute ethanol and deionized water to remove unreacted reagents and impurities, then redispersed in 50 mL of $CHCl_3$, to which excess red-emitting hydrophobic CdSe/ZnS QD dispersion was added, and the mixture was sonicated for 30 min to obtain a clear and transparent solution. The complex was washed repeatedly with chloroform to remove unattached CdSe/ZnS QDs. Afterwards, the obtained MF@CdSe/ZnS NFs were properly dried under N_2 flow and redispersed in 20 mL of $CHCl_3$, which contained 2 mg of branched PEI, under sonication for 30 min. After centrifugation and washing in deionized water, the MF@CdSe/ZnS@PEI NFs were dispersed in the PBS solution (0.01 M, pH = 7.4) and stored in a refrigerator for later use.

2.4. Preparation Procedures of Ab_2-MF@CdSe/ZnS@PEI

Anti-β-HCG was assembled to form bioconjugates with MF@CdSe/ZnS@PEI via EDC/NHS chemical cross-linking. Firstly, the freshly prepared MF@CdSe/ZnS@PEI NFs (1 mg/mL) were dispersed in PBS solution (0.01 M, pH = 7.4), and a Sulfo-NHS solution with a concentration of 5 mg/mL was added and shaken at room temperature for 4 h. After the reaction was completed, MF@CdSe/ZnS@PEI NFs were washed several times with ethanol and water to remove excess PEI and impurities and then redispersed in MES buffer solution (0.01 M, pH = 6.0) for use. Next, the carboxyl-modified MF@CdSe/ZnS@PEI NFs were dispersed into a 0.5 mL MES buffer solution (0.01 M, pH = 6.0) to prepare a concentration of 2 mg/mL, followed by adding 4 mg EDC (Energy Chemical) and 6 mg Sulfo-NHS (Energy Chemical). The above mixture was shaken and reacted at room temperature for half an hour. Afterwards, 100 μg of Anti-β-HCG (Ab_2) was added and incubated at 4 °C overnight. Finally, the Ab_2-MF@CdSe/ZnS@PEI bioconjugates were collected by centrifugation and washed several times with HEPES buffer solution (0.01 M,

pH = 7.4) containing 1% BSA to remove unbound proteins. It was then redispersed in HEPES buffer solution and stored in the refrigerator.

2.5. Fabrication Procedures of the MF@CdSe/ZnS@PEI-ICTS

The pretreatment steps and preparation processes of MF@CdSe/ZnS@PEI-ICTS are basically consistent with those reported in our previous literature [40,41]. The test strip is mainly composed of four parts: a pre-treated sample pad, an NC membrane, an absorbent pad, and a black polyvinyl chloride (PVC) back card. Anti-α-HCG (Linc-Bio, Ab_1, 1.5 mg/mL) and goat anti-mouse IgG antibodies (Linc-Bio, 1 mg/mL) were applied to NC membranes by fiber pen to constitute the test (T) and control (C) lines, respectively. The prepared NC membranes were then dried at 37 °C overnight. Finally, the sample pad, NC membrane, and absorbent pad were sequentially connected and laid on a black PVC backing card, each adjacent section overlapping about 1–2 mm, and finally cut into pieces with a width of about 3.9 mm by a chopper.

2.6. Detection of HCG Standard Samples with the MF@CdSe/ZnS@PEI-ICTS

Firstly, HCG standard solutions of different concentrations (0, 0.01, 0.1, 1, 10, 50, 100, 200, and 500 mIU/mL) were prepared, and 40 µL of each concentration solution and 20 µL of Ab_2-MF@CdSe/ZnS@PEI NFs were premixed. After that, the mixture was added dropwise to the sample pad of the test strip. Each concentration was tested 3 times in parallel. After 15 min, under the excitation of a 365 nm UV lamp, qualitative results can be obtained by observing the red band on the test strip. Photographs were taken with a mobile phone camera for qualitative measurement, and the captured images were processed using ImageJ software version 1.50d to obtain the intensities of the T- and C-lines [42,43].

3. Results and Discussion

3.1. Preparation and Characterization of MF@CdSe/ZnS@PEI NFs

As shown in Figure 2a,b, the MF NFs prepared in this work consist of many nanosheets, which are interconnected to form an open structure with a size of about 260 nm. $Mg(OAc)_2{\cdot}4H_2O$ and $FeCl_3{\cdot}6H_2O$ were used as precursors, and ethylene glycol was used as a solvent. MF NFs were synthesized by the solvothermal method in an autoclave [44–46]. In addition, we applied Fourier transform-infrared spectroscopy (FT-IR), X-ray diffraction (XRD), and X-ray photoelectron spectroscopy (XPS) methods (Figure 3a,c and Figure S5) to characterize the MF NFs prepared in this work, and the results showed that they were consistent with the basic characteristics of LDH-like materials [35,36]. MF@CdSe/ZnS NFs can be obtained by sonicating oil-soluble CdSe/ZnS quantum dots (7 nm, Figure S1) of uniform size with SH-MF in chloroform solution for 30 min. As shown in Figure 2c, MF NFs as carriers can bond high-density loaded hydrophobic CdSe/ZnS QDs via Cd-S covalent bonding. After the MF@CdSe/ZnS NFs were modified with an optimized amount of branched PEI, we employed energy dispersive X-ray spectroscopy (EDS) elemental mapping to investigate its elemental composition. From Figure 2d–l, the elements contained in the MF@CdSe/ZnS@PEI NFs composite were all determined, which can prove the successful preparation of MF@CdSe/ZnS@PEI. In Figure 3a, the characteristic peaks located at 2920 cm^{-1} (-CH_2), 1458 cm^{-1} (-CH_2), and 1380 cm^{-1} (-CH_3) are consistent with bare CdSe/ZnS QDs (Figure S2), indicating that MF@CdSe/ZnS NFs were successfully prepared. For MF@CdSe/ZnS@PEI, the characteristic peaks of amino groups at 3448 cm^{-1} and 1640 cm^{-1} indicate that PEI exists on the surface of MF@CdSe/ZnS NFs, implying the successful introduction of amino functional groups. The UV-vis absorption data in Figure 3b show that the absorption peaks of CdSe/ZnS QDs, MF@CdSe/ZnS, and MF@CdSe/ZnS@PEI are all around 625 nm, which indicates that QDs loaded into MF NFs do not exhibit an obvious absorption peak shift, and the properties are not affected. As shown in Figure 3c, XRD measurements were applied to characterize the crystal composition of MF NFs and MF@CdSe/ZnS NFs. As indicated by the black lines in Figure 3c, MF NFs have five main peaks located at 9.26°, 22.1°, 34.1°, 38.0°, and 59.7°, respectively, and the corresponding

crystal planes are (003), (006), (012), (015), and (110) [36]. The three broad peaks located at 26.1°, 43.3°, and 50.6° in the figure correspond to the (111), (220), and (311) plane diffractions, respectively. These crystal plane data are generally consistent with the cubic sphalerite structure of bulk CdSe (JCPDS file No. 88–2346) [47–49]. By observing Figure S3, the chemical shift peaks of the methylene belonging to 3-MPTMS can be determined, which are 17.30, 20.48, and 32.92 ppm, respectively, which indicates that PEI has been successfully modified to the MF@CdSe/ZnS NFs. Meanwhile, it can be seen from Figure S4 that with the loading of hydrophobic QDs, the zeta potential value changes from negative to positive; this result further proves that the loading of hydrophobic QDs changes the surface potential of MF NFs. We performed fluorescence characterization of hydrophobic CdSe/ZnS QDs, MF@CdSe/ZnS, and MF@CdSe/ZnS@PEI NFs using a spectrofluorometer. Characterization results show that the emission wavelength of CdSe/ZnS QDs is 642 nm, while the emission wavelengths of MF@CdSe/ZnS and MF@CdSe/ZnS@PEI NFs are 658 and 662 nm, respectively. Compared with CdSe/ZnS QDs, the emission wavelengths of MF@CdSe/ZnS and MF@CdSe/ZnS@PEI NFs are about 20 nm redshifted we think this may be caused by the larger overall particle size of oily quantum dots loaded by MF NFs. XPS was used to characterize the main elemental composition of MF@CdSe/ZnS NFs, and it can be seen from Figure 4a that C, O, Mg, Cd, and Zn elements were determined. High-resolution XPS spectra of C 1s, O 1s, Mg 2p, Cd 3d, and Zn 2p are recorded in Figure 4b–f. Among them, three peaks with binding energies of about 284.6 eV, 286.1 eV, and 288.0 eV can be seen in the C 1s spectrum, which correspond to the C-C coordination of the surface adventitious carbon and the C-O and C = O in the acetate anion, respectively. For O 1s, the peak at 531.4 eV in the spectrum can be attributed to the C-O and C=O bonds of oleic acid, while 532.0 eV corresponds to the bidentate carboxylate. Two peaks belonging to the Mg-OH (49.0 eV) and Mg-O (50.0 eV) bonds can be found in the spectrum of Mg 2p, respectively. Figure 4e shows that the characteristic doublets of the Cd 3d spectrum at 404.8 eV and 411.7 eV come from Cd $3d_{5/2}$ and Cd $3d_{3/2}$, respectively. Among them, the binding energy of Cd $3d_{5/2}$ is consistent with the value reported in the literature (the binding energy of bulk CdSe is 405.6 eV). Figure 4f shows the noisy signal of Zn 2p, which was deconvolved into two components. The peak at 1020.6 eV is related to Zn $2p_{3/2}$, and 1044.0 eV is related to Zn $2p_{1/2}$.

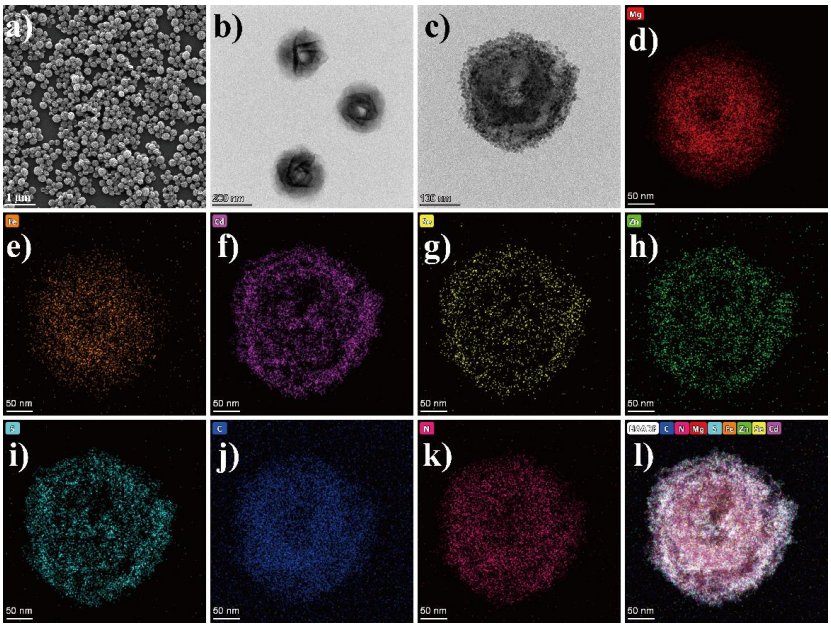

Figure 2. (**a**,**b**) Field emission scanning electron microscope (SEM) and transmission electron microscope (TEM) images of Mg/Fe LDH NFs. (**c**) TEM images of MF@CdSe/ZnS@PEI NFs. (**d**–**l**) EDS elemental mapping images of MF@CdSe/ZnS@PEI NFs.

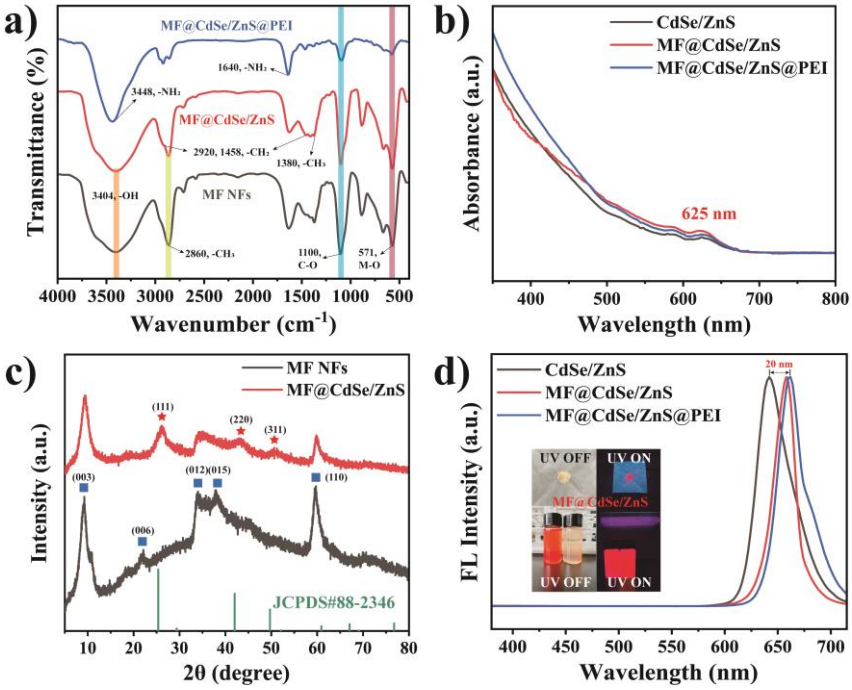

Figure 3. (**a**) Fourier transform-infrared spectra of Mg/Fe LDH NFs, MF@CdSe/ZnS NFs, and MF@CdSe/ZnS@PEI NFs. (**b**) UV-vis absorption spectra of hydrophobic CdSe/ZnS QDs, MF@CdSe/ZnS NFs, and MF@CdSe/ZnS@PEI NFs. (**c**) XRD patterns of Mg/Fe LDH NFs and MF@CdSe/ZnS NFs. (**d**) Fluorescence spectra of hydrophobic CdSe/ZnS QDs, MF@CdSe/ZnS, and MF@CdSe/ZnS@PEI NFs. (Inset is the fluorescence photo of MF@CdSe/ZnS@PEI NFs solid and dispersed in water).

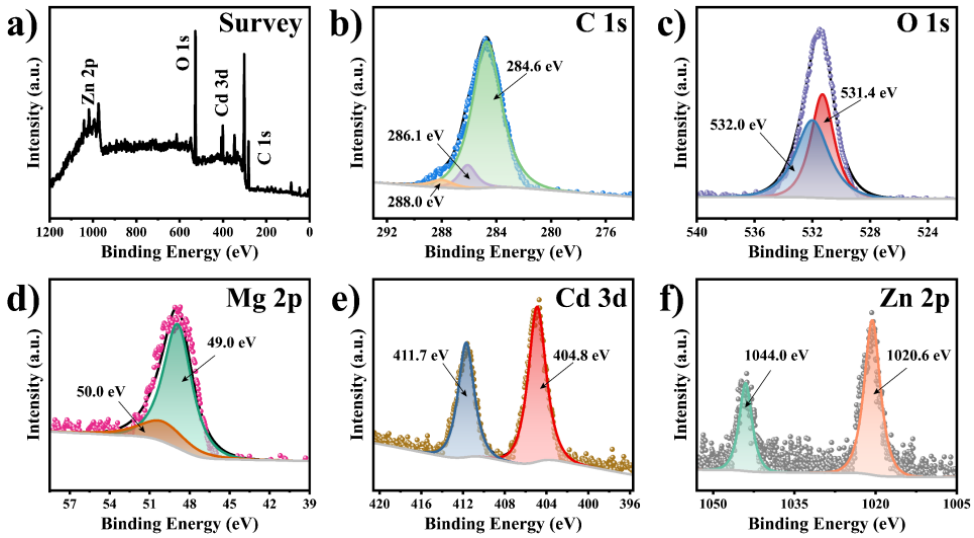

Figure 4. (**a**) XPS survey spectrum of MF@CdSe/ZnS NFs. (**b**–**f**) High-resolution XPS spectra of C 1s, O 1s, Mg 2p, Cd 3d, and Zn 2p.

3.2. Performance of MF@CdSe/ZnS@PEI-ICTS for HCG Detection

Before using MF@CdSe/ZnS@PEI-ICTS to detect different concentrations of HCG standards, optimizing the concentration of branched PEI coated with MF@CdSe/ZnS is critical to achieve the detection. It can be seen from Figure S6 that when the concentration exceeds 0.5 mg/mL, it will cause the MF@CdSe/ZnS NFs to exhibit mutual adhesion. The branched PEI concentration used in this work was finally determined to be 0.1 mg/mL. MF@CdSe/ZnS@PEI-ICTS is based on the independent immunoreactions of T and C probes

to realize the fluorescence detection of HCG with different concentration gradients. The capture antibody Ab_1, which specifically reacts with the antigen HCG, is painted on the T-line, and goat anti-mouse immunoglobulin is painted on the C-line. The reaction on the T-line is based on a probe-coupled antibody-antigen-coated antibody double-antibody sandwich immunoreaction (i.e., Ab_2-MF@CdSe/ZnS@PEI-HCG-Ab_1), and the reaction on the C-line is based on direct immunoreactivity with probe-conjugated secondary antibody and goat anti-mouse immunoglobulin (i.e., Ab_2-MF@CdSe/ZnS@PEI-IgG). When Ab_2-MF@CdSe/ZnS@PEI was mixed with HCG samples of different concentrations and then dropped on the sample pad, the droplets were chromatographed on the NC membrane under capillary action. If there is HCG in the solution, Ab_2-MF@CdSe/ZnS@PEI-HCG will react with Ab_1 to form Ab_2-MF@CdSe/ZnS@PEI-HCG-Ab_1. When the droplet continued to flow to the C-line, Ab_2-MF@CdSe/ZnS@PEI that was not bound to Ab_1 would have a direct immune reaction with goat anti-mouse IgG to form Ab_2-MF@CdSe/ZnS@PEI-IgG. The qualitative results of MF@CdSe/ZnS@PEI-ICTS were obtained based on the visual observation of the line color on the NC membrane under a 365 nm UV lamp. After about 15 min, as shown in Figure 5a, the NC membranes of all test strips can display the C-line normally, which proves that the detection results are valid. Visual inspection of the test strips under UV light gives a limit of detection (LOD) of approximately 0.1 mIU/mL. At the same time, with the increase in the concentration of HCG standard solution, the red fluorescence color of the T-line on the NC membranes gradually deepened, which means that more Ab_2-MF@CdSe/ZnS@PEI was captured on the T-line. With the assistance of ImageJ software version 1.50d, we can obtain the grayscale signal intensities of the detection and control lines on the NC membrane. To compensate for potential intensity variations caused by acquisition conditions such as lighting and camera settings, background subtraction is required, and the ratio of T-line intensity to C-line intensity (T/C) is used in this work to quantify the signal (Figure S7). First, the RGB image taken by the phone is converted to an 8-bit grayscale image type and inverted. Then, the rectangular box tool is used to measure the average intensity of the T-line, C-line, and background areas. Subtract the average intensity of the background area from the average intensity of the T- and C-lines, take the T/C value as the ordinate, and take the HCG concentration as the abscissa, and a linear relationship between the two can be fitted (Figure 5b). The linear regression equation is $y = 0.0957 \times -0.139$ ($R^2 = 0.98$). In addition, we also verified the potential of MF@CdSe/ZnS@PEI-ICTS in clinical application by HCG standard sample addition and recovery experiments. Healthy human serum was spiked with different concentrations of HCG (10, 50, and 100 mIU/mL), and the experiment was repeated three times on test strips. We selected a batch of serum from healthy people, added different concentrations of HCG standard samples (i.e., 10, 50, and 100 mIU/mL) to them, and after incubation with Ab_2-MF@CdSe/ZnS@PEI, applied them to MF@CdSe/ZnS@PEI-ICTS to detect the recovery rate of standard addition. As shown in Table S1, the spiked recoveries were between 90.48 and 116.1%, and the coefficient of variation was below 15%, which indicated that MF@CdSe/ZnS@PEI-ICTS has the potential to be used in the analysis of clinical samples [50]. In addition, we list and compare the analytical performance of different HCG detection methods in Table S2. Compared with electrochemical and electrochemiluminescence methods, the sensitivity of MF@CdSe/ZnS@PEI-ICTS appears to be poor. However, as a POCT tool, MF@CdSe/ZnS@PEI-ICTS still has the advantages of being fast and convenient, and it has a wider linear range and a lower detection limit than similar testing methods. Finally, we selected four biomarkers (AFP, CA125, CA199, and CEA) at a concentration of 1 μg/mL to evaluate and validate the cross-reactivity of MF@CdSe/ZnS@PEI-ICTS. The results are shown in Figure S8. Except for HCG, other biomarkers could not generate corresponding red fluorescence on the T-line, which proves that MF@CdSe/ZnS@PEI-ICTS has good selectivity and low cross-reactivity.

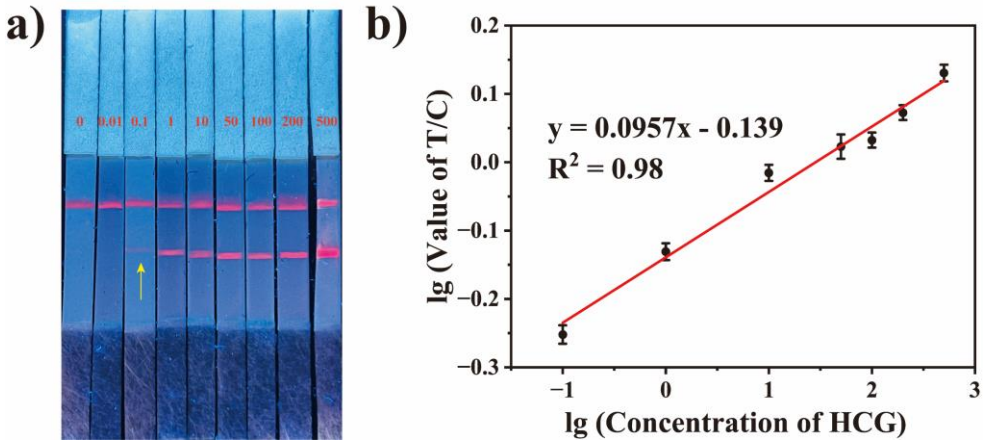

Figure 5. (**a**) Image of the MF@CdSe/ZnS@PEI-ICTS when detecting HCG standard solution (0, 0.01, 0.1, 1, 10, 50, 100, 200, and 500 mIU/mL). (**b**) Linear response of MF@CdSe/ZnS@PEI-ICTS for detection of HCG.

4. Conclusions

In conclusion, a novel fluorescent signal reporter that can be used in ICTS was prepared by implanting hydrophobic CdSe/ZnS QDs into Mg/Fe LDH nanoflowers in one step through the metal-thiol covalent bonds in the organic phase. By modifying the MF@ CdSe/ZnS with branched PEI, which not only improved its dispersion in the buffer but also introduced amino functional groups on the surface of the reporter to facilitate subsequent antibody conjugation. Under optimal experimental conditions, HCG was used as the model analyte with a linear detection range from 0.1 to 500 mIU/mL and a visual limit of detection of 0.1 mIU/mL. Compared with commercial pregnancy diagnostic strips, the addition of high-density hydrophobic CdSe/ZnS QDs greatly improved the detection sensitivity of HCG. The potential for practical application was validated by detecting HCG in spiked healthy human serum, showing overall recoveries of between 90.48 and 116.1% with coefficients of variation between 3.66 and 12.91%. Moreover, the experimental results found that MF@CdSe/ZnS@PEI-ICTS has good selectivity and little cross-reactivity with AFP, CA125, CA199, and CEA. This work preliminarily explores the possibility of Mg/Fe LDH NFs as signal carriers in ICTS, which greatly improves the practicality of ICTS.

Supplementary Materials: The following supporting information can be downloaded at: https://www.mdpi.com/article/10.3390/chemosensors11020114/s1, Figure S1: TEM images of oil-soluble, red-emitting CdSe/ZnS QDs. Figure S2: FT-IR spectra of oil-soluble, red-emitting CdSe/ZnS QDs. Figure S3: Solid-state ^{13}C CP/MAS NMR spectrum of SH-MF NFs. Figure S4: ζ-potential results of MF NFs, hydrophobic CdSe/ZnS QDs, MF@CdSe/ZnS, and MF@CdSe/ZnS@PEI NFs. Figure S5: XPS spectra of (a) C 1s, (b) Mg 2p, (c) Fe 2p, and (d) O 1s of MF NFs. Figure S6: MF@CdSe/ZnS NFs coated with different concentrations of branched PEI. Figure S7. Image processing procedures of MF@CdSe/ZnS@PEI-ICTS. Step 1: convert the photo taken by the mobile phone into an 8-bit grayscale image. Step 2: obtain the inverse image of the grayscale image by using the Invert option. Step 3: define the average intensity of the T-line, C-line, and background regions in the inverse image. Figure S8: Cross-reactivity of MF@CdSe/ZnS@PEI-ICTS for different biomarkers. Table S1: Recovery efficiency and coefficient of variation (CV) for the MF@CdSe/ZnS@PEI-ICTS for HCG (mIU/mL) to be detected in human serum samples (n = 3). Table S2. Summary of HCG detection with some different detection methods [51–56].

Author Contributions: Methodology, investigation, writing—original draft, writing—review and editing, visualization, H.L.; data curation and methodology, Q.Z.; methodology, N.B.; conceptualization, methodology, resources, funding acquisition, writing—review and editing, supervision, S.-N.D. All authors have read and agreed to the published version of the manuscript.

Funding: This work was supported by the National Key Research and Development Program of China (2017YFA0700404) and the National Natural Science Foundation of China (22174015).

Informed Consent Statement: Not applicable.

Data Availability Statement: Not applicable.

Conflicts of Interest: The authors declare no conflict of interest.

References

1. Wu, L.; Qu, X. Cancer biomarker detection: Recent achievements and challenges. *Chem. Soc. Rev.* **2015**, *44*, 2963–2997. [CrossRef] [PubMed]
2. Mahmoudi, T.; de la Guardia, M.; Baradaran, B. Lateral flow assays towards point-of-care cancer detection: A review of current progress and future trends. *TrAC Trends Anal. Chem.* **2020**, *125*, 115842. [CrossRef]
3. Plotz, C.M.; Singer, J.M. The latex fixation test: II. Results in rheumatoid arthritis. *Am. J. Med.* **1956**, *21*, 893–896. [CrossRef]
4. Brucker, M.C.; Macmullen, N.J. What's New in Pregnancy Tests. *J. Obstet. Gynecol. Neonatal Nurs.* **1985**, *14*, 353–359. [CrossRef] [PubMed]
5. Fang, C.-C.; Chou, C.-C.; Yang, Y.-Q.; Wei-Kai, T.; Wang, Y.-T.; Chan, Y.-H. Multiplexed Detection of Tumor Markers with Multicolor Polymer Dot-Based Immunochromatography Test Strip. *Anal. Chem.* **2018**, *90*, 2134–2140. [CrossRef] [PubMed]
6. He, H.; Liu, B.; Wen, S.; Liao, J.; Lin, G.; Zhou, J.; Jin, D. Quantitative Lateral Flow Strip Sensor Using Highly Doped Upconversion Nanoparticles. *Anal. Chem.* **2018**, *90*, 12356–12360. [CrossRef] [PubMed]
7. Liu, X.; Wang, K.; Cao, B.; Shen, L.; Ke, X.; Cui, D.; Zhong, C.; Li, W. Multifunctional Nano-Sunflowers with Color-Magnetic-Raman Properties for Multimodal Lateral Flow Immunoassay. *Anal. Chem.* **2021**, *93*, 3626–3634. [CrossRef] [PubMed]
8. Liu, G.; Lin, Y.-Y.; Wang, J.; Wu, H.; Wai, C.M.; Lin, Y. Disposable Electrochemical Immunosensor Diagnosis Device Based on Nanoparticle Probe and Immunochromatographic Strip. *Anal. Chem.* **2007**, *79*, 7644–7653. [CrossRef] [PubMed]
9. Jia, J.; Ao, L.; Luo, Y.; Liao, T.; Huang, L.; Zhuo, D.; Jiang, C.; Wang, J.; Hu, J. Quantum dots assembly enhanced and dual-antigen sandwich structured lateral flow immunoassay of SARS-CoV-2 antibody with simultaneously high sensitivity and specificity. *Biosens. Bioelectron.* **2022**, *198*, 113810. [CrossRef] [PubMed]
10. Huang, L.; Liao, T.; Wang, J.; Ao, L.; Su, W.; Hu, J. Brilliant Pitaya-Type Silica Colloids with Central–Radial and High-Density Quantum Dots Incorporation for Ultrasensitive Fluorescence Immunoassays. *Adv. Funct. Mater.* **2018**, *28*, 1705380. [CrossRef]
11. Wang, T.; Zhuang, J.; Lynch, J.; Chen, O.; Wang, Z.; Wang, X.; LaMontagne, D.; Wu, H.; Wang, Z.; Cao, Y.C. Self-Assembled Colloidal Superparticles from Nanorods. *Science* **2012**, *338*, 358–363. [CrossRef] [PubMed]
12. Xia, Y.; Nguyen, T.D.; Yang, M.; Lee, B.; Santos, A.; Podsiadlo, P.; Tang, Z.; Glotzer, S.C.; Kotov, N.A. Self-assembly of self-limiting monodisperse supraparticles from polydisperse nanoparticles. *Nat. Nanotechnol.* **2011**, *6*, 580–587. [CrossRef]
13. Yi, C.; Zhang, S.; Webb, K.T.; Nie, Z. Anisotropic Self-Assembly of Hairy Inorganic Nanoparticles. *Acc. Chem. Res.* **2017**, *50*, 12–21. [CrossRef]
14. Foubert, A.; Beloglazova, N.V.; De Saeger, S. Comparative study of colloidal gold and quantum dots as labels for multiplex screening tests for multi-mycotoxin detection. *Anal. Chim. Acta* **2017**, *955*, 48–57. [CrossRef]
15. Deng, H.; Liu, Q.; Wang, X.; Huang, R.; Liu, H.; Lin, Q.; Zhou, X.; Xing, D. Quantum dots-labeled strip biosensor for rapid and sensitive detection of microRNA based on target-recycled nonenzymatic amplification strategy. *Biosens. Bioelectron.* **2017**, *87*, 931–940. [CrossRef] [PubMed]
16. Gong, X.; Cai, J.; Zhang, B.; Zhao, Q.; Piao, J.; Peng, W.; Gao, W.; Zhou, D.; Zhao, M.; Chang, J. A review of fluorescent signal-based lateral flow immunochromatographic strips. *J. Mater. Chem. B* **2017**, *5*, 5079–5091. [CrossRef] [PubMed]
17. Yang, H.; Li, D.; He, R.; Guo, Q.; Wang, K.; Zhang, X.; Huang, P.; Cui, D. A Novel Quantum Dots–Based Point of Care Test for Syphilis. *Nanoscale Res. Lett.* **2010**, *5*, 875. [CrossRef] [PubMed]
18. Hu, J.; Zhang, Z.-L.; Wen, C.-Y.; Tang, M.; Wu, L.-L.; Liu, C.; Zhu, L.; Pang, D.-W. Sensitive and Quantitative Detection of C-Reaction Protein Based on Immunofluorescent Nanospheres Coupled with Lateral Flow Test Strip. *Anal. Chem.* **2016**, *88*, 6577–6584. [CrossRef]
19. Gao, F.; Lei, C.; Liu, Y.; Song, H.; Kong, Y.; Wan, J.; Yu, C. Rational Design of Dendritic Mesoporous Silica Nanoparticles' Surface Chemistry for Quantum Dot Enrichment and an Ultrasensitive Lateral Flow Immunoassay. *ACS Appl. Mater. Interfaces* **2021**, *13*, 21507–21515. [CrossRef] [PubMed]
20. Li, X.; Li, W.; Yang, Q.; Gong, X.; Guo, W.; Dong, C.; Liu, J.; Xuan, L.; Chang, J. Rapid and Quantitative Detection of Prostate Specific Antigen with a Quantum Dot Nanobeads-Based Immunochromatography Test Strip. *ACS Appl. Mater. Interfaces* **2014**, *6*, 6406–6414. [CrossRef] [PubMed]
21. Duan, H.; Huang, X.; Shao, Y.; Zheng, L.; Guo, L.; Xiong, Y. Size-Dependent Immunochromatographic Assay with Quantum Dot Nanobeads for Sensitive and Quantitative Detection of Ochratoxin A in Corn. *Anal. Chem.* **2017**, *89*, 7062–7068. [CrossRef] [PubMed]
22. Joumaa, N.; Lansalot, M.; Théretz, A.; Elaissari, A.; Sukhanova, A.; Artemyev, M.; Nabiev, I.; Cohen, J.H.M. Synthesis of Quantum Dot-Tagged Submicrometer Polystyrene Particles by Miniemulsion Polymerization. *Langmuir* **2006**, *22*, 1810–1816. [CrossRef]
23. Wang, C.; Yang, X.; Gu, B.; Liu, H.; Zhou, Z.; Shi, L.; Cheng, X.; Wang, S. Sensitive and Simultaneous Detection of SARS-CoV-2-Specific IgM/IgG Using Lateral Flow Immunoassay Based on Dual-Mode Quantum Dot Nanobeads. *Anal. Chem.* **2020**, *92*, 15542–15549. [CrossRef] [PubMed]
24. Bai, F.; Wang, D.; Huo, Z.; Chen, W.; Liu, L.; Liang, X.; Chen, C.; Wang, X.; Peng, Q.; Li, Y. A Versatile Bottom-up Assembly Approach to Colloidal Spheres from Nanocrystals. *Angew. Chem. Int. Ed.* **2007**, *46*, 6650–6653. [CrossRef]

25. Zhuang, J.; Wu, H.; Yang, Y.; Cao, Y.C. Controlling Colloidal Superparticle Growth Through Solvophobic Interactions. *Angew. Chem. Int. Ed.* **2008**, *47*, 2208–2212. [CrossRef]
26. Gao, X.; Nie, S. Doping Mesoporous Materials with Multicolor Quantum Dots. *J. Phys. Chem. B* **2003**, *107*, 11575–11578. [CrossRef]
27. Yang, F.; Skripka, A.; Tabatabaei, M.S.; Hong, S.H.; Ren, F.; Huang, Y.; Oh, J.K.; Martel, S.; Liu, X.; Vetrone, F.; et al. Magnetic Photoluminescent Nanoplatform Built from Large-Pore Mesoporous Silica. *Chem. Mater.* **2019**, *31*, 3201–3210. [CrossRef]
28. Huang, L.; Wu, Q.; Wang, J.; Foda, M.; Liu, J.; Cai, K.; Han, H. A brilliant sandwich type fluorescent nanostructure incorporating a compact quantum dot layer and versatile silica substrates. *Chem. Commun.* **2014**, *50*, 2896–2899. [CrossRef]
29. Lu, Z.; Gao, C.; Zhang, Q.; Chi, M.; Howe, J.Y.; Yin, Y. Direct Assembly of Hydrophobic Nanoparticles to Multifunctional Structures. *Nano Lett.* **2011**, *11*, 3404–3412. [CrossRef]
30. Wu, Q.; Chen, L.; Huang, L.; Wang, J.; Liu, J.; Hu, C.; Han, H. Quantum dots decorated gold nanorod as fluorescent-plasmonic dual-modal contrasts agent for cancer imaging. *Biosens. Bioelectron.* **2015**, *74*, 16–23. [CrossRef]
31. Wang, Q.; O'Hare, D. Recent Advances in the Synthesis and Application of Layered Double Hydroxide (LDH) Nanosheets. *Chem. Rev.* **2012**, *112*, 4124–4155. [CrossRef] [PubMed]
32. Song, L.; Shi, W.; Lu, C. Confinement Effect in Layered Double Hydroxide Nanoreactor: Improved Optical Sensing Selectivity. *Anal. Chem.* **2016**, *88*, 8188–8193. [CrossRef]
33. Yu, Y.; Lu, C.; Zhang, M. Gold Nanoclusters@Ru(bpy)3^{2+}-Layered Double Hydroxide Ultrathin Film as a Cathodic Electrochemiluminescence Resonance Energy Transfer Probe. *Anal. Chem.* **2015**, *87*, 8026–8032. [CrossRef] [PubMed]
34. Zong, Y.; Li, K.; Tian, R.; Lin, Y.; Lu, C. Highly dispersed layered double oxide hollow spheres with sufficient active sites for adsorption of methyl blue. *Nanoscale* **2018**, *10*, 23191–23197. [CrossRef]
35. Mubarak, M.; Islam, M.S.; Yoon, D.-Y.; Lee, J.H.; Park, H.J.; Bae, J.-S.; Lee, H.-J. Flower-like Mg/Fe-layered double oxide nanospheres with ultrahigh adsorption efficiency for anionic organic dyes. *Colloids Surf. A Physicochem. Eng. Asp.* **2021**, *618*, 126446. [CrossRef]
36. Mubarak, M.; Jeon, H.; Islam, M.S.; Yoon, C.; Bae, J.-S.; Hwang, S.-J.; Choi, W.S.; Lee, H.-J. One-pot synthesis of layered double hydroxide hollow nanospheres with ultrafast removal efficiency for heavy metal ions and organic contaminants. *Chemosphere* **2018**, *201*, 676–686. [CrossRef] [PubMed]
37. Yang, Q.; Gong, X.; Song, T.; Yang, J.; Zhu, S.; Li, Y.; Cui, Y.; Li, Y.; Zhang, B.; Chang, J. Quantum dot-based immunochromatography test strip for rapid, quantitative and sensitive detection of alpha fetoprotein. *Biosens. Bioelectron.* **2011**, *30*, 145–150. [CrossRef]
38. Chen, Z.; Liang, R.; Guo, X.; Liang, J.; Deng, Q.; Li, M.; An, T.; Liu, T.; Wu, Y. Simultaneous quantitation of cytokeratin-19 fragment and carcinoembryonic antigen in human serum via quantum dot-doped nanoparticles. *Biosens. Bioelectron.* **2017**, *91*, 60–65. [CrossRef]
39. Cho, J.; Jung, Y.K.; Lee, J.-K. Kinetic studies on the formation of various II–VI semiconductor nanocrystals and synthesis of gradient alloy quantum dots emitting in the entire visible range. *J. Mater. Chem.* **2012**, *22*, 10827–10833. [CrossRef]
40. Xu, L.-D.; Zhang, Q.; Ding, S.-N.; Xu, J.-J.; Chen, H.-Y. Ultrasensitive Detection of Severe Fever with Thrombocytopenia Syndrome Virus Based on Immunofluorescent Carbon Dots/SiO_2 Nanosphere-Based Lateral Flow Assay. *ACS Omega* **2019**, *4*, 21431–21438. [CrossRef] [PubMed]
41. Xu, L.D.; Zhu, J.; Ding, S.N. Immunoassay of SARS-CoV-2 nucleocapsid proteins using novel red emission-enhanced carbon dot-based silica spheres. *Analyst* **2021**, *146*, 5055–5060. [CrossRef]
42. Kim, M.; Kim, M.S.; Kweon, S.H.; Jeong, S.; Kang, M.H.; Kim, M.I.; Lee, J.; Doh, J. Simple and Sensitive Point-of-Care Bioassay System Based on Hierarchically Structured Enzyme-Mimetic Nanoparticles. *Adv. Healthc. Mater.* **2015**, *4*, 1311–1316. [CrossRef]
43. Kim, M.S.; Kweon, S.H.; Cho, S.; An, S.S.A.; Kim, M.I.; Doh, J.; Lee, J. Pt-Decorated Magnetic Nanozymes for Facile and Sensitive Point-of-Care Bioassay. *ACS Appl. Mater. Interfaces* **2017**, *9*, 35133–35140. [CrossRef]
44. Huang, P.; Liu, J.; Wei, F.; Zhu, Y.; Wang, X.; Cao, C.; Song, W. Size-selective adsorption of anionic dyes induced by the layer space in layered double hydroxide hollow microspheres. *Mater. Chem. Front.* **2017**, *1*, 1550–1555. [CrossRef]
45. Géraud, E.; Rafqah, S.; Sarakha, M.; Forano, C.; Prevot, V.; Leroux, F. Three Dimensionally Ordered Macroporous Layered Double Hydroxides: Preparation by Templated Impregnation/Coprecipitation and Pattern Stability upon Calcination. *Chem. Mater.* **2008**, *20*, 1116–1125. [CrossRef]
46. Wang, B.; Wu, H.; Yu, L.; Xu, R.; Lim, T.-T.; Lou, X.W. Template-free Formation of Uniform Urchin-like α-FeOOH Hollow Spheres with Superior Capability for Water Treatment. *Adv. Mater.* **2012**, *24*, 1111–1116. [CrossRef]
47. Kim, K.M.; Jeon, J.H.; Kim, Y.Y.; Lee, H.K.; Park, O.O.; Wang, D.H. Effects of ligand exchanged CdSe quantum dot interlayer for inverted organic solar cells. *Org. Electron.* **2015**, *25*, 44–49. [CrossRef]
48. Granados-Oliveros, G.; Pineros, B.S.G.; Calderon, F.G.O. CdSe/ZnS quantum dots capped with oleic acid and L-glutathione: Structural properties and application in detection of Hg^{2+}. *J. Mol. Struct.* **2022**, *1254*, 132293. [CrossRef]
49. Cingarapu, S.; Yang, Z.; Sorensen, C.M.; Klabunde, K.J. Synthesis of CdSe/ZnS and CdTe/ZnS Quantum Dots: Refined Digestive Ripening. *J. Nanomater.* **2012**, *2012*, 312087. [CrossRef]
50. Jin, Y.; Chen, Q.; Luo, S.; He, L.; Fan, R.; Zhang, S.; Yang, C.; Chen, Y. Dual near-infrared fluorescence-based lateral flow immunosensor for the detection of zearalenone and deoxynivalenol in maize. *Food Chem.* **2021**, *336*, 127718. [CrossRef]
51. Zhang, A.; Guo, W.; Ke, H.; Zhang, X.; Zhang, H.; Huang, C.; Yang, D.; Jia, N.; Cui, D. Sandwich-format ECL immunosensor based on Au star@BSA-Luminol nanocomposites for determination of human chorionic gonadotropin. *Biosens. Bioelectron.* **2018**, *101*, 219–226. [CrossRef] [PubMed]

52. Hong, G.; Zhang, D.; He, Y.; Yang, Y.; Chen, P.; Yang, H.; Zhou, Z.; Liu, Y.; Wang, Y. New photothermal immunoassay of human chorionic gonadotropin using Prussian blue nanoparticle-based photothermal conversion. *Anal. Bioanal. Chem.* **2019**, *411*, 6837–6845. [CrossRef]
53. Zhang, T.; Wang, H.-B.; Zhong, Z.-T.; Li, C.-Q.; Chen, W.; Liu, B.; Zhao, Y.-D. A smartphone-based rapid quantitative detection platform for lateral flow strip of human chorionic gonadotropin with optimized image algorithm. *Microchem. J.* **2020**, *157*, 105038. [CrossRef]
54. Wang, X.; Xue, C.-H.; Yang, D.; Jia, S.-T.; Ding, Y.-R.; Lei, L.; Gao, K.-Y.; Jia, T.-T. Modification of a nitrocellulose membrane with nanofibers for sensitivity enhancement in lateral flow test strips. *RSC Adv.* **2021**, *11*, 26493–26501. [CrossRef]
55. Danthanarayana, A.N.; Finley, E.; Vu, B.; Kourentzi, K.; Willson, R.C.; Brgoch, J. A multicolor multiplex lateral flow assay for high-sensitivity analyte detection using persistent luminescent nanophosphors. *Anal. Methods* **2020**, *12*, 272–280. [CrossRef]
56. Liang, H.; Ning, G.; Wang, L.; Li, C.; Zheng, J.; Zeng, J.; Zhao, H.; Li, C.-P. Covalent Framework Particles Modified with MnO_2 Nanosheets and Au Nanoparticles as Electrochemical Immunosensors for Human Chorionic Gonadotropin. *ACS Appl. Nano Mater.* **2021**, *4*, 4593–4601. [CrossRef]